Nuclear Instruments and Methods in Physics Research A 374 (1996) 254–268

ELSEVIER

NUCLEAR INSTRUMENTS & METHODS IN PHYSICS RESEARCH Section A

Shielding calculations for a 250 MeV hospital-based proton accelerator

Stefano Agosteo[a,*], Gianluigi Arduini[b,1], Giorgio Bodei[a], Stefano Monti[c], Franca Padoani[c], Marco Silari[d], Renato Tinti[c], Giuliana Tromba[e]

[a]*Dipartimento di Ingegneria Nucleare, Politecnico di Milano, via Ponzio 34/3, 20133 Milano, Italy*
[b]*Fondazione Italiana Ricerca sul Cancro, via Corridoni 7, 20122 Milano, Italy*
[c]*ENEA, ERG-FISS-FIRE, via Martiri di Monte Sole 4, 40129 Bologna, Italy*
[d]*Consiglio Nazionale delle Ricerche, Istituto Tecnologie Biomediche Avanzate, via Ampère 56, I-20131, Milano, Italy*
[e]*Sincrotrone ("ELETTRA") Trieste, Padriciano 99, 34012 Trieste, Italy*

Received 20 July 1995; revised form received 27 December 1995

Abstract

The accelerator shields (250 MeV protons, 400 MeV/u $^{16}O^{8+}$ ions) and treatment rooms of the Hadrontherapy Centre, a hospital-based facility under design in Italy, were determined by means of Monte Carlo calculations. The LCS and FLUKA codes were employed, together with analytical estimates carried out by making use of empirical formulas from the literature, and the results compared. In the case of 250 MeV protons a 250 cm thick concrete wall ensures an annual dose equivalent lower than 2 mSv in the environments adjacent to the accelerator room. The best ceiling thickness was found to be 200 cm for a unitary occupancy factor. The photon dose equivalent beyond the concrete shield was also estimated using the LCS code. In the case of ions the shield thickness was calculated using empirical formulas from the literature; the concrete thicknesses calculated for protons should ensure the required dose equivalent when some local shields are added. Monte Carlo calculations of the treatment room shielding were also carried out using the FLUKA code.

1. Introduction

The Hadrontherapy Centre is a proposed hospital-based facility which will be built in the north of Italy [1]. The term "hadrontherapy" has been adopted to collectively indicate cancer radiation therapy with hadron beams, i.e. heavy charged particles (protons and light ions) and neutrons. The main accelerator is a synchrotron capable of accelerating H^- ions up to 250 MeV and, as a possible upgrade, fully stripped ions (up to $^{16}O^{8+}$) up to 400 MeV/u [2]. Protons will be extracted by charge exchange [3]. The required vacuum in the synchrotron doughnut is about 10^{-10} Torr, to avoid the stripping of the second electron of the H^- ion in the atomic collisions with the residual gas molecules [4]. The possibility of using the resonant technique to accelerate and extract protons is also foreseen, as a backup capability in case of vacuum problems. Two separate linacs will inject H^- and light ions into the synchrotron at 11 MeV and 3 MeV/u, respectively. Since only a modest beam intensity is necessary for therapy (of the order of a few 10^{10} protons s^{-1} and about 10^9 $^{16}O^{8+}$ ions s^{-1}), only a modest average beam current needs to be injected and accelerated in the synchrotron. The exceeding beam current, available from the injectors, is planned to be used for alternative purposes, e.g., radionuclide production (RNP) for PET diagnostics and neutron production on a beryllium target for boron neutron capture therapy (BNCT) [5]. The Centre for Oncological Hadrontherapy will consist of two buildings: an underground, heavily shielded area (the "bunker") housing the accelerators and the treatment rooms, and a surface building above ground with conventional facilities and office space. The bunker has a surface area of about 3500 m^2. Two treatment rooms will be equipped with an isocentric gantry. This unit allows the 360° rotation of the terminal tract of the beam line around the patient in order to vary the direction of irradiation, as is done in conventional radiotherapy. Fig. 1a shows a plan view of the facility. The bunker includes:

1. two treatment rooms equipped with an isocentric gantry capable of transporting protons up to 250 MeV;

* Corresponding author. Tel. +39 2 2399 6318, fax +39 2 2399 6309, e-mail 2cesne4@ipmcc3.polimi.it.
[1] Present address: CERN, 1211 Geneve 23, Switzerland.

PII S0168-9002(96)00017-4

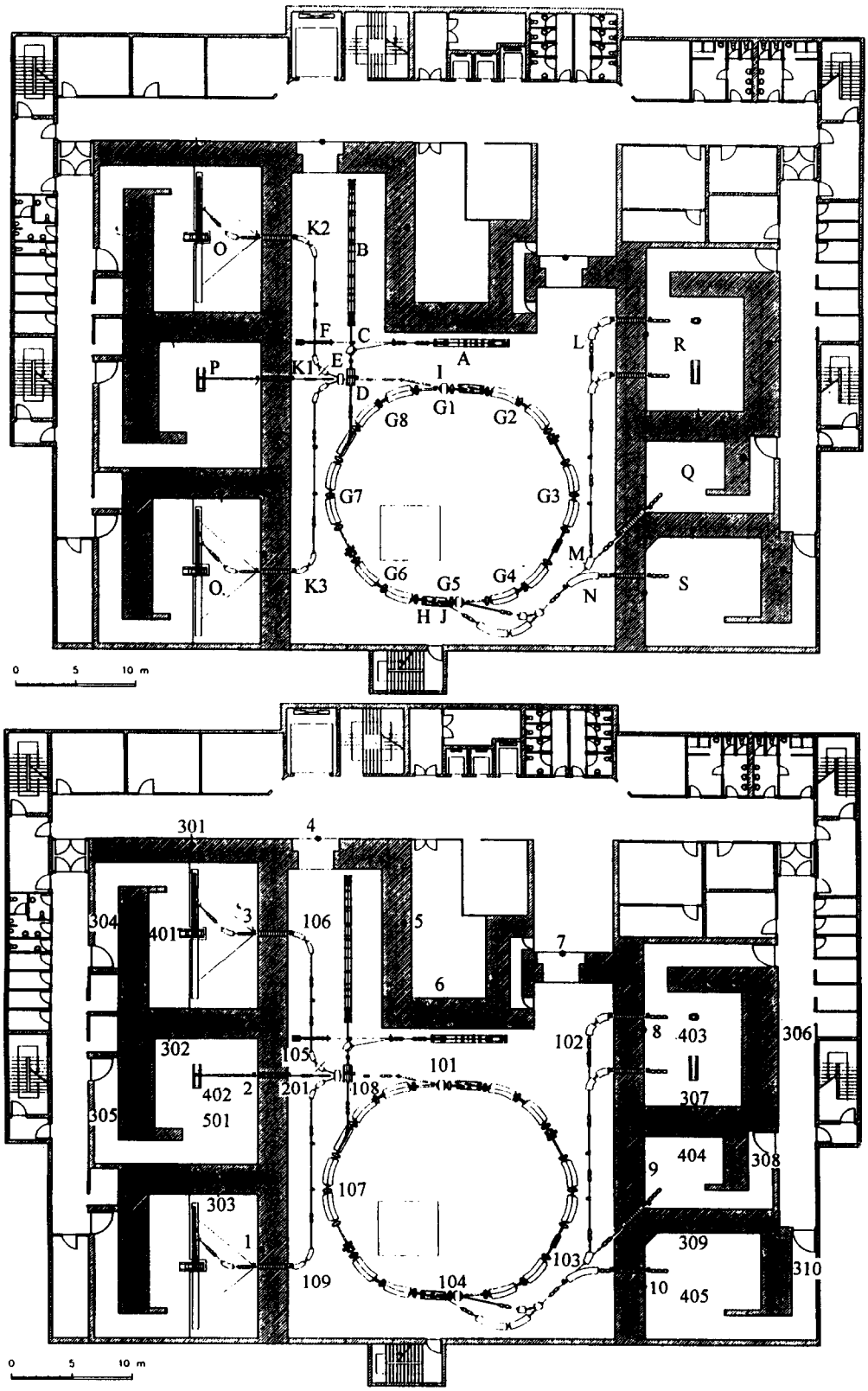

Fig. 1. (a) Plan view of the Hadrontherapy Centre. The beam loss sources are indicated. (b) Plan view of the Hadrontherapy Centre. The positions at which the dose equivalent was estimated are indicated.

2. one treatment room equipped with one horizontal and one vertical (downward) beam, also for 250 MeV proton beams;
3. one room equipped with two horizontal beam lines, one for eye tumour irradiations and one mainly devoted to the treatment of head and neck tumours;
4. one room with one horizontal beam for experimental activities with both protons and light ions (dosimetry, radiobiology, calibrations, etc.);
5. one room devoted to future light ion treatments;
6. two smaller rooms served by the 11 MeV proton beam from the injector, one for the production of positron-emitting radionuclides for PET diagnostics (^{11}C, ^{13}N, ^{15}O and ^{18}F), the other for BNCT thermal neutron production.

Forward and transverse shielding of proton accelerators is the subject of a fairly extensive literature [6–15]. Both analytical estimates based on the Moyer formula [6,8] and Monte Carlo simulations were carried out by taking into consideration the effect of concrete and iron slabs. Experimental verifications are reported in Refs. [11,14], while Ref. [13] focuses on the photon dose behind the shields of high energy accelerators (100 GeV protons). However, an estimate of the shields aimed at the particular structure of the Hadrontherapy Centre is of primary importance for meeting the two opposite requirements of ensuring doses below the recommended limits in the requested environments and reducing the construction costs. To this end, a set of Monte Carlo simulations was performed by considering the real geometry of the designed facility and the various radiation sources inside the accelerator room and the treatment rooms. In this way the shielding of neutrons scattering on the room walls was also taken into account.

A dose equivalent of 2 mSv per year (corresponding to 1 μSv/h for personnel working full-time for 2000 h/year) is the limit chosen taking into account the ICRP-60 [16] recommendations (i.e., 20 mSv/year) and an additional safety factor of 10. This factor is justified by the possible future increase of the radiation weighting factors (formerly quality factor) by ICRP and by the fact that the facility will be built in a town, in a highly populated area. The radiological impact on the external environment has to be practically zero.

The following occupancy factors were assumed:

- corridors: 1/4;
- treatment rooms: 1;
- control room: 1;
- facilities: 1;
- experimental rooms: 1;
- corridor under the accelerator vault for servicing gantries: 1/16;
- building above the accelerator vault: 1.

The first step of the present work was to estimate the expected sources of beam loss at the accelerator complex (i.e, the injectors, the synchrotron, the beam transport lines, the isocentric gantries and the patients). The probability and frequency of the beam losses, the use factors of the facility and the time spent by the workers around the machine were considered in order to accurately evaluate the source strength. The maximum accelerator energies were conservatively taken into account. Subsequently, in the case of 250 MeV protons, the shield constraints were determined in the real geometry for every source both with analytical calculations and Monte Carlo simulations. The accelerator room and treatment rooms were separately considered. Both the LCS [17] and the FLUKA [18] codes were employed. In particular, as proton interactions take place in the magnets, the energy and angular distributions of neutrons emitted by an iron target bombarded with 250 MeV protons were determined with both codes and the results were accurately compared. Subsequently, shielding was treated with both codes, paying attention to the consistency of the results. As both codes proved to be reliable in the context of the present work, the simulations referring to some environments (e.g. the treatment rooms) were performed by only one code. No energy cutoff and variance reduction techniques were employed in either code.

The contribution of photons from the de-excitation of the residual nuclei produced by proton interactions and in neutron absorption reactions mainly occurring in the walls of the room was also investigated using Monte Carlo simulations.

Unfortunately, the available Monte Carlo codes do not treat ions with secondary particle production and transport, mainly since there is a lack of reliable nuclear models. Consequently some assumptions were made in this case, as discussed in Section 3, in order to check that the barriers evaluated for protons would be satisfactory in the case of ions. Otherwise, additional local shields will have to be installed. The calculations relating to the necessary shield when an upgrading to ion acceleration is carried out refer only to ^{16}O.

It should be noted that the present work refers to a particular facility. However, as discussed in Section 7, the results are completely in agreement with those estimated in the literature for a general situation.

2. Beam loss sources

This section provides an estimate of the expected sources of beam losses at the accelerator complex, to be used as a basic assumption for calculating the shielding structures. The estimates made here assume the maximum energy of the accelerated particles and should therefore be considered as conservative. The beam loss data are reported in Table 1 and are identified by the same letters shown in Fig. 1a. The positions where the dose equivalent was estimated are shown in Fig. 1b. The data on efficiency

Table 1
Beam loss sources

Loss source	Particle	Maximum energy [MeV/u]	Average beam current [particle A[a]]	Target material	Loss factor [%]	Duty factor [h/day]
A) H^-/proton linac	H^-/protons	11	100×10^{-6}	Cu	20	4.7
B) Light ion linac	^{16}O	0.250	370×10^{-9}	Cu	10	2
		0.850	330×10^{-9}		55	2
		3	150×10^{-9}		45	2
C) Beam line selection–injection, BNCT and RNP	H^-/protons	11	80×10^{-6}	Fe	10	4.7
D) Injection line for light ions	^{16}O	3	82×10^{-9}	Fe	10	2
E) Linac beam dump	H^-/protons	11	4.6×10^{-6}	C	100	8
	^{16}O	3	74×10^{-9}	C	100	2
F) Beam line, low energy – high current	H^-/protons	11	72×10^{-6}	Fe	10	4.2
G) Synchrotron	H^-/protons	11	28×10^{-9}	Fe	15	7
		250	28×10^{-9}	Fe	5	7
	^{16}O	3	0.89×10^{-9}	Fe	5	2
		400	0.89×10^{-9}	Fe	5	2
H) Synchrotron beam dump	H^-/protons	250	25×10^{-9}	Fe	100	0.25
	^{16}O	400	0.71×10^{-9}	Fe	100	0.15
I) H^- extraction	H^-	250	22×10^{-9}	Fe	10	3
J) H^-, proton and light ion resonant extraction	H^-/protons	250	22×10^{-9}	Fe	10	4
	^{16}O	400	0.71×10^{-9}	Fe	20	2
K) Beam transfer to gantries and to horiz. and vert. beam rooms	protons	250	20×10^{-9}	Fe	10	3
L) Transfer line to horiz. beam treatment room	protons	250	20×10^{-9}	Fe	10	1
M) Beam transfer line to experimental room	H^-/protons	250	20×10^{-9}	Fe	10	3
	^{16}O	400	0.57×10^{-9}	Fe	20	1
N) Light ion beam transfer line	^{16}O	400	0.57×10^{-9}	Fe	10	1
O) Isocentric gantry room	protons	250	18×10^{-9}	Fe	5	1
				Cu	45	1
				H_2O or tissue	50	1
P) Fixed horiz. and vert. beam room	protons	250	18×10^{-9}	Fe	5	1
				Cu	45	1
				H_2O or tissue	50	1
Q) Experimental room	protons	250	18×10^{-9}	Cu	20	3
				H_2O or tissue	80	1
	^{16}O	400	0.51×10^{-9}	Cu	20	1
				H_2O or tissue	80	1
R) Horiz. beam treatment room	protons	70 (30%)	18×10^{-9}	Fe	5	1
		250 (70%)	18×10^{-9}	Cu	45	1
				H_2O or tissue	50	1
S) Light ion treatment room	^{16}O	400	0.51×10^{-9}	Fe	5	1
				H_2O or tissue	95	1
T) BNCT treatment room	protons	11	100×10^{-6}	Be	100	2
U) RNP room	protons	11	20×10^{-6}	O (50%)	100	4
				N (50%)	100	4

[a] Particle A is a unit for expressing the current intensity divided by the charge (in electronic charge unit) of the ions. For protons 1 particle A obviously coincides with 1 A.

for acceleration and transport of particles in the various components of the accelerator system were partly taken from Ref. [19]. The beam height above floor level is 1.15 m.

The considered loss conditions refer to a normal operating mode. In the case of a failure of a subsystem (e.g., one of the power supplies of the synchrotron dipoles) leading to an accidental loss of the beam either in the ring

or along one of the transfer lines to the treatment rooms, the safety system will intervene and abort the machine operation in the next acceleration cycle (e.g., in less than 0.5 s).

Losses referring to the synchrotron (which include injection, RF capture and acceleration) are assumed to be uniformly distributed around the ring. Such losses are divided into the following two classes:

1. losses occurring in the course of the injection process (including RF capture) plus those possibly due to collisional detachment of the second electron of the H^- ion following an interaction with the molecules of the residual gas in the vacuum chamber: these occur at low energies (11 MeV) and account for about 15% of the overall figure of 20% as given below;
2. losses occurring in the course of the acceleration process: these are not expected to exceed 5% of the overall figure of 20%; the maximum energy of 250 MeV is considered. Such a radiation source can be considered more or less uniformly distributed around the machine circumference. In practice the beam will most likely be lost in correspondence to the dipoles; since there are six dipole pairs, the overall loss would be subdivided along 10 m arcs centered at each of these pairs, each one contributing about 17% to the overall loss factor. For the shielding calculations, the beam losses can be concentrated at the centre of each dipole pair and should be taken in a tangential direction with respect to the synchrotron ring at that point. The simulations described in the following considered both this latter assumption and a source distributed along one half of the ring. The same applies for ions.

The beam dump for fast beam abort (point H in Fig. 1a) is placed inside the synchrotron. This source loss physically coincides with point J of Table 1 and Fig. 1a. In the final design it may not be placed here, but substituted by two dumps external to the machine, one in each beam line. Nevertheless, it is unlikely that this would change the shielding requirements.

The maximum energies reported in Table 1 for the light ion linac (point B) refer to its different acceleration sections. In the horizontal beam treatment room (point R), eye irradiation will be performed with 70 MeV protons for 30% of the overall time. Copper as target material (points O, P and R) is assumed where the use of a passive beam spreading device (collimator) is foreseen for dose shaping. H_2O or soft tissue account for the beam dumped in the patient.

As discussed below, the present work refers only to the shielding of the accelerator room and the treatment rooms, so that some beam loss sources (e.g, BNCT and RNP) reported in Table 1 will not be discussed here. Moreover, the shielding was calculated for the maximum beam energy, so that other sources with lower energies (such as the injectors) will not be discussed.

3. Analytical calculations

Much theory and experimental data concerning neutron production in different thick target materials bombarded by protons of various energies can be found in the literature. Some semiempirical expressions were extrapolated (e.g. see Refs. [6,8,15]) to calculate the neutron dose equivalent in different directions beyond the concrete slabs.

Several data on neutron production by the interaction of heavy ions with matter are also available [20–31]. However, most of them are concerned either with measurements of neutron yields produced by ions with energies (up to 50 MeV/u) lower than those of interest in the present work (up to 400 MeV/u) or with experimental data that cannot be applied for general purposes.

As already mentioned, the available Monte Carlo codes do not treat the production and transport of secondary particles in ion interactions because of the lack of reliable nuclear models. For example, in Ref. [29], ^{4}He interactions with matter in the energy range between 100 MeV/u and 800 MeV/u, are simulated with the HETC/KFA code by means of two independent interacting pairs made up of a neutron and a proton. The comparison of the simulation results with experimental data shows that the code overestimates the neutron yield in the forward direction and underestimates the neutron production at large angles. In spite of these discrepancies, in Ref. [29] is pointed out that the calculated absolute yield above 10 MeV is in accordance with the experimental values. Moreover, in the same reference the ratio of neutron yield for ^{4}He ions to that for protons is almost equal to the number of ^{4}He nucleons is emphasized.

As alternative models were not available for the specific case of the present work (^{16}O ions at 400 MeV/u), the analytical calculations of the ion facility were performed by considering the neutron emission induced by an ion of mass A and energy E (MeV/u) equivalent to that produced by the interaction of A protons of energy E (MeV). The estimate of the neutron yield is performed by assuming that the full beam is stopped in the target (''thick target'') and that the different ranges of ions, with respect to protons, do not affect the total neutron emission. These assumptions are clearly a rough approximation of the actual physical process and this approach is only intended to give very preliminary information on the shielding requirements for ion operation.

With the above hypotheses, the calculations for the heavy ion facility can be performed by using the same semiempirical equations as for protons. The general expression for the evaluation of shielding thickness $x(\theta)$ (in m), θ being the polar angle of the secondary particles, can be derived from the Moyer model [8] as a function of the

Table 2
Source terms $H(\theta)$ and attenuation coefficients $\mu(\theta)$ for neutrons in ordinary concrete for the transverse and the forward directions [15]

Ion	Energy	Component	$H(\theta)$ [Sv m^2 per ion]	$\mu(\theta)$ [m^{-1}]
Proton	20 MeV	Forward and transverse	3×10^{-17}	7.9
Proton	250 MeV	Forward	10^{-14}	2.4
Proton	250 MeV	Transverse	1.8×10^{-15}	3.1
^{16}O	400 MeV/u	Forward	$16 \times 1.35 \times 10^{-14}$	1.7
^{16}O	400 MeV/u	Transverse	16×10^{-14}	2.5

beam current, the barrier use factor, the beam loss scenario and the dose equivalent limit in the environments adjacent to the accelerator and treatment rooms:

$$x(\theta) = \frac{1}{\mu(\theta)} \ln\left(k \frac{H(\theta)\, I\, p_{\text{loss}} t_{\text{loss}} U\, T}{D_{\max} r^2}\right), \quad (1)$$

where $\mu(\theta)$ (m^{-1}) is the mean attenuation coefficient of neutron shield material in the direction θ; $D_{\max}$ (Sv h^{-1}) is the limiting dose equivalent rate behind the shield (1 μSv h^{-1} in this case); r (m) is the distance between the source and the point of interest (obviously $r > x$, including the barrier); $H(\theta)$ (Sv m^2 per ion) is the source term along the direction θ; I (ions/s) is the particle current; p_{loss} ($0 < p_{\text{loss}} \leq 1$) is the beam loss fraction; t_{loss} (h/day) is the duty factor; T is the occupancy factor; U ($0 < U \leq 1$) is the use factor of the barrier; k is a constant taking into account the different time units used in the formula.

Table 2 shows the source terms and the attenuation coefficients in ordinary concrete in the forward and transverse directions for protons at 20 MeV and 250 MeV, taken from Ref. [15]. Source terms for ^{16}O ions were obtained by multiplying the data reported in Ref. [15] by a factor of 16 for 400 MeV protons. The results of the analytical calculations are reported in Table 2a. The data reported in Table 2a show that some shield thickness referring to the proton facility (e.g. those referring to sources G3, G4, H, Q) are likely to be sufficient when the

Table 2a
Shield thiknesses calculated with the analytical method for each beam loss source

Beam loss source (see Fig. 1a)	Forward shielding		Lateral Shielding	
	r (m) see expression (1)	Calculated thickness (m)	r (m) see expression (1)	Calculated thickness (m)
G3 (250 MeV protons)	19	1.5	6	1.8
G4 (250 MeV protons)	13	2.4		
G3 (400 MeV/u ^{16}O)	19	1	6	1.6
G4 (400 MeV/u ^{16}O)	13	2.3		
H (250 Mev protons)	16	3		
H (400 Mev/u ^{16}O)	16	2.3		
I	15	2.8	7	2.1
J (250 MeV protons)	16	2.9		
J (400 MeV/u ^{16}O)	16	3.6		
K	11	2.4	6.5	2.1
L	4.5	2	6.5	2.4
M (250 MeV protons)	6.5	3.4	4.5	2.3
M (400 MeV/u ^{16}O)	6.5	3.7	4.5	2.3
N	9.5	3.3	4.5	2.3
O (40% of the time vertical pointing downwards)			8.5	2
O (20% horizontal from left to right)	8.5	3		
O (20% horizontal from right to left)	8.5	2.7		
O (20% other directions)	8.5	2.4		
P	6.5	3	6.5	2.2
Q (250 MeV protons)	12	3.3	5.5	2.9
Q (400 MeV/u ^{16}O)	12	3.3	5.5	3
R	6.5	3.2	5.5	2.5
S	8.5	3.8	6.5	2.9

ion upgrade is carried out, while some local shields should be added in the proximity of some beam loss sources (e.g. sources J and M).

4. Source term simulations

Iron and copper thick targets were considered in a cylindrical geometry, as the actual design of the synchrotron magnets, of the beam transport lines and of the collimators of the beam delivery systems has yet to be defined. Consequently the self-shielding effect of thicker secondary particle sources was omitted, thus giving rise to a conservative estimate.

A set of simulations was performed in order to determine the target dimensions ensuring the most unfavorable combination of the neutron yield and the double differential distribution. Larger target dimensions generally correspond to higher neutron yields and lower average neutron energies. The target thickness was fixed, taking into account the 250 MeV proton range in the considered material, while the radius was chosen referring to the neutron energy spectrum.

Table 3 reports the neutron and photon yields for different radii of the iron target, calculated with the two codes. Fig. 2 shows the neutron yield (for energies larger than 20 MeV) at various polar angles for different iron target radii, as calculated with FLUKA. It should be noted that at polar angles between 60° and 120° the effect of lateral self-absorption with increasing target radius is emphasized; at 90° the neutron yield depression is stronger and in particular, values lower than those referring to 180° can be observed. An analogous effect can be deduced from the experimental data and the simulation results reported in Ref. [32]. Radii lower than 5.8 cm were not investigated as they are not realistic when simulating accelerator dipoles. Notwithstanding the absolute yield increases with radius,

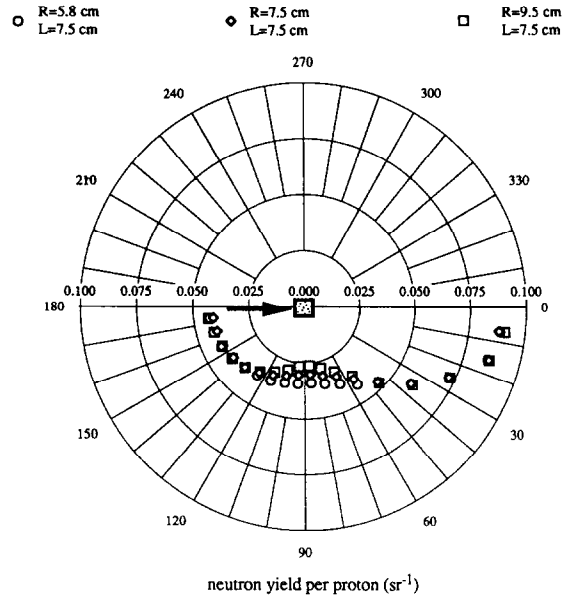

Fig. 2. Polar diagram of the neutron yields above 20 MeV per incident proton at various polar angles for different iron target radii, as calculated with FLUKA.

as shown in Table 3, priority was given to high energy neutrons. A radius of 5.8 cm was chosen for the reference iron target. Fig. 3 shows the double differential distribution of neutrons emitted by the reference target in some angular bins, calculated with LCS and FLUKA and compared with the experimental data of Ref. [32]. The differences between the two codes are more evident at large polar angles. This can be attributed to the lack of the preequilibrium model in the available LCS version. Nevertheless, it can be assumed that this difference has a negligible effect on shielding calculations. Fig. 4 shows the double differential

Table 3
Neutron and photon yields (neutron per proton) for cylindrical iron targets of variable radius bombarded by 250 MeV protons

Target Thickness [cm]	Target radius [cm]	Absolute neutron yield (LCS)	Absolute neutron yield (FLUKA)	Absolute photon yield (LCS)
7.5	5.8	0.833	0.768	0.209
7.5	7.5	0.837	–	0.207
7.5	9.5	0.842	–	0.215
7.5	11.5	0.845	–	0.213
7.5	13.5	0.846	–	0.213

Table 4
Source terms used in the simulations

Target material	Density [g cm^{-3}]	250 MeV proton range [cm]	Target radius [cm]	Target thickness [cm]	Absolute neutron yield
Fe	7.87	6.85	5.8	7.5	0.833
Cu	8.95	6.27	5.0	6.5	0.994[a]
H_2O	1.00	38	20.0	20.0	0.200[a]

[a]Calculated for neutron energies above 20 MeV.

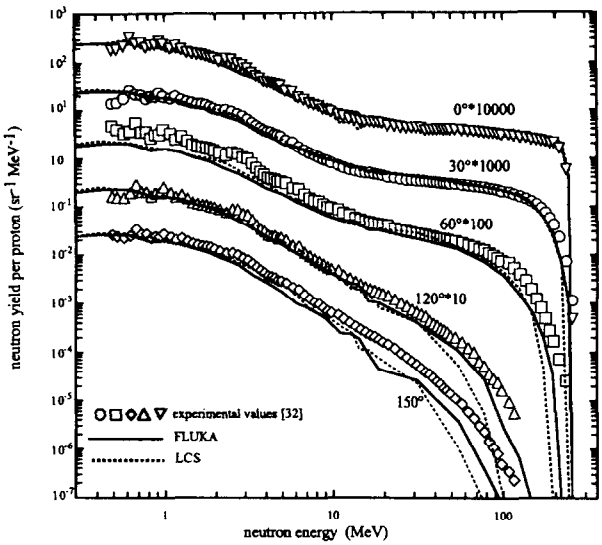

Fig. 3. Double differential distribution of neutrons produced by 250 MeV proton bombardment of an iron target (5.8 cm radius, 7.5 cm thick), calculated with LCS and FLUKA and compared with the data of Ref. [32] (referring to an 8.0 cm × 8.0 cm iron target).

distribution of neutrons at all angles, as calculated with FLUKA. The same procedure was adopted to optimize the copper target dimensions.

The chosen water target dimensions maximize the "hardness" of the neutron energy distribution. Consequently, a thin target has been considered in this conservative approach, where the attention was mainly focused on neutron spectrum instead of neutron yield. The final source terms and target dimensions used in the simulations are given in Table 4. Fig. 5 shows the angular distributions calculated with FLUKA for the iron, copper and water targets.

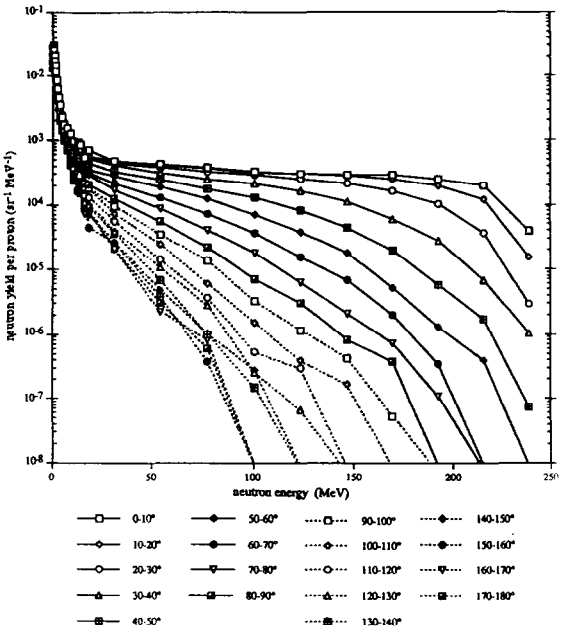

Fig. 4. Double differential distribution at all angles of neutrons produced by a thick iron target bombarded by 250 MeV protons (calculated with FLUKA).

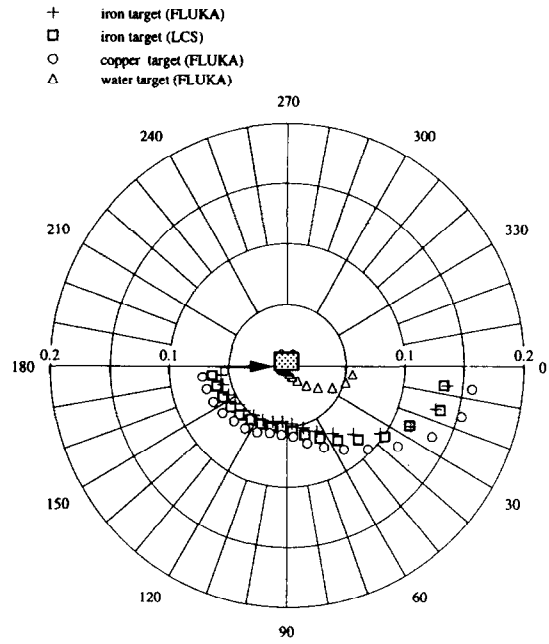

Fig. 5. Polar diagram of the neutron angular distribution following 250 MeV proton bombardment of iron (calculated with FLUKA and LCS), copper and water (calculated with FLUKA) reference targets (see text).

De-excitation photon production in iron was also considered in the LCS simulations. Table 3 also reports the absolute photon yields for the considered target dimensions. Fig. 6 shows the energy distribution of the de-excitation photons calculated with LCS averaged over all angles. The angular distribution of the photon yield shows a minimum at about 90° polar angle, probably due to the larger dimensions of the iron target in that direction.

5. LCS shielding simulations

The simulations performed with the LCS code refer to the accelerator room shielding and are based on the real geometry of the designed facility. Geometry splitting cannot be performed in the available version of LAHET (the part of LCS treating particle transport above 20 MeV) and therefore much computing time was necessary. The considered shielding material is concrete TSF-5.5 (density 2.31 g cm^{-3}) with the following weight fractions: oxygen 40.81%, calcium 32.54%, carbon 17.43%, silicon 3.43%,

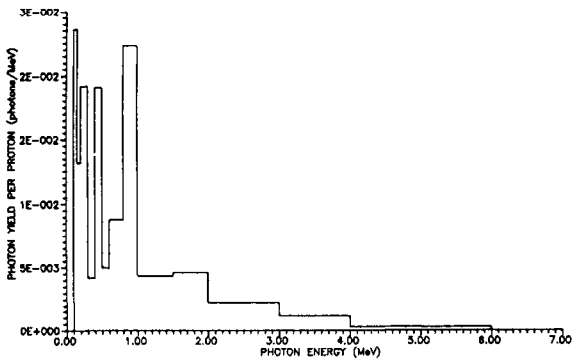

Fig. 6. Energy distribution of the de-excitation photons produced by 250 MeV proton bombardment of an iron target (calculated with LCS).

magnesium 3.25%, aluminum 1.16%, iron 0.76%, hydrogen 0.62%. In the available LCS libraries for elastic scattering, calcium and magnesium are not present. Therefore, in the input file of the LAHET code, the elastic cross sections of these elements were substituted with those of elements with a larger mass number, i.e. titanium and aluminium respectively. A similar method was adopted in Ref. [10]. In the LCS code system, neutrons are transported below 20 MeV by MCNP, whose associated libraries include a very extensive series of elements. Therefore, the exact concrete composition was defined for these energies, thus accurately treating the prompt gamma ray production in thermal neutron absorption reactions. In particular, the ENDL85 cross section file of the Lawrence Livermore Laboratory, was used. No energy cutoff was set either for neutrons or for photons. The neutron dose equivalent rate behind the shield was calculated by means of the fluence to dose equivalent conversion factors determined in Ref. [33].

A preliminary set of simulations was performed to evaluate the shield thickness, whose effect on the real geometry was verified in a second step. The dose equivalent attenuation was estimated in cells delimited by fictitious plane surfaces inside the shielding walls, simulated 400 cm thick, of the real accelerator room geometry. Table 5 reports the results at various depths in the forward direction, considering one of the synchrotron beam loss sources (see Fig. 1a, point G1). In this case a 250 MeV proton beam impinging on the base of the iron cylinder described in the previous section was simulated. It should be noted that at a depth of 250 cm, the dose equivalent rate is 0.76 $\mu Sv\ h^{-1}$. This is lower than the limiting value of 1 $\mu Sv\ h^{-1}$, therefore 250 cm is the thickness chosen for the verifications described in the following.

The simulations described above scored the neutron fluence inside the concrete shield, where the fluence to dose equivalent conversion factors are employed. The neutron fluence inside the shield may be overestimated

Table 5
Neutron dose equivalent at various depths in the shield in the forward direction for an iron target at the position G1 (see Fig. 1a)

Depth [cm]	Neutron dose equivalent per proton [Sv]	Neutron dose equivalent rate [$\mu Sv\ h^{-1}$]
0	6.02×10^{-17}	236.88
0–50	3.42×10^{-17}	134.73
50–100	6.45×10^{-18}	25.47
100–130	2.89×10^{-18}	11.38
130–160	1.37×10^{-18}	5.41
160–190	7.44×10^{-19}	2.93
190–220	4.01×10^{-19}	1.58
220–250	1.94×10^{-19}	0.76
250–280	1.07×10^{-19}	0.42
280–310	8.34×10^{-20}	0.33
310–340	5.28×10^{-20}	0.21
340–370	1.67×10^{-20}	0.07
370–400	1.85×10^{-21}	0.08
400	5.71×10^{-22}	0.02

with respect to that calculated behind a slab of thickness equal to the scoring depth, as a result of neutrons backscattering and diffusing in the concrete itself. Therefore the simulations described above are useful for dose attenuation problems, but the correct estimate of the dose equivalent in the environment behind the shield should be performed by taking into account the real thickness, as will be stressed in Section 7. To this purpose the real geometry of the accelerator room with walls 250 cm thick was considered in the simulations described in the following.

In all the simulations the effect of air and of the equipment that will be installed in the rooms (i.e. the synchrotron, the beam transfer lines, etc.) was omitted. As already mentioned, the beam loss sources of the synchrotron and of the beam lines were assumed to be localized at the same positions of the dipole magnets. The source positions are indicated in Fig. 1a. The effect of every source was studied in separate simulations, in which a 250 MeV proton beam impinging on an iron target of the reference dimensions was considered together with the real geometry of the facility.

The neutron fluence averaged in void cells 1 cm thick placed immediately behind the shield was scored in various energy groups. The dose equivalent was estimated with the fluence to dose equivalent conversion factors mentioned above. As already mentioned the wall thickness is 250 cm, while the floor and ceiling were tentatively set to 160 and 150 cm, respectively. As the resulting dose equivalent at some positions above the ceiling was larger than the limiting value of 2 $mSv\ y^{-1}$, the ceiling shielding was optimized in a separate set of simulations, aimed at an accurate spatial estimate of the dose equivalent in the various environments above it. Consequently the neutron transport load and therefore the computing time were reduced. In the following, the simulations referring to

different beam loss sources will be separately described for better evidence.

5.1. Synchrotron

The beam loss around the synchrotron was treated as the superposition of eight separate sources localized at the dipole positions (G1–G8, Fig. 1a). The contribution of each source behind the shields was calculated with separate simulations. The errors of the resulting data (referring to a single source contribution) behind the shields are lower than 15%. At some scoring positions (e.g. position 3 with source G3, see Figs. 1a and 1b, at large distances and in a transverse direction with respect to the considered source, the error was between 30 and 40%. However, these non-accurate values were taken into account as an estimate of the low contribution of the considered source in the considered position. A better accuracy would have involved a very high computing time, unjustifiable in the technical context of the present work. Moreover the quantity of interest is the total contribution of the beam loss sources in the environments adjacent to the accelerator room and thus the relative error of the values obtained by adding more accurate and larger contributions of the other sources will obviously be lower. The results are given in Table 6. The zero values refer to a null contribution in the neutron fluence scoring.

5.2. Synchrotron beam dump

The synchrotron beam dump (H in Table 1 and Fig. 1a) is directed towards the ground (no occupied area below it). Its contribution behind the accelerator room walls is negligible.

5.3. Beam extraction

The contribution of the beam extraction systems (I and J in Table 1 and Fig. 1a) can be estimated from the results of the simulations referring to the synchrotron as discussed above, as they coincide with points G1 and G5.

5.4. Beam transfer lines

As already mentioned these sources (K, L, M and N in Table 1) were concentrated at the positions of the bending magnets. Thus the losses along the beam transport to the gantries and to the horizontal and vertical beam rooms (K) were subdivided into three different concentrated sources, as shown in Fig. 1a. It should be mentioned that the irradiation will alternatively be carried out in each treatment room. The total loss factor of sources K and L (20%) was equally subdivided among the localized sources K1, K2, K3 and L, thus resulting in 5% for each one.

Table 7 reports the dose equivalent rates for the beam loss sources described above. It should be noted that at three positions (2, 7 and 10, in bold in the table) the dose limit of 1 $\mu Sv\,h^{-1}$ is exceeded. The resulting maximum dose equivalent of 4 $\mu Sv\,h^{-1}$ occurs in a treatment room. However, the effect of local shielding in the proximity of the more intense sources of beam loss was taken into account and will be discussed in the following. It should be mentioned, as a further result of this set of simulations, that the neutron yield in the room walls due to (n,xn) reactions on concrete is about 0.15 neutrons per source proton. This quantity has to be compared with the neutron yield in the iron target, estimated to be 0.82 neutrons per source proton in Section 4 (see Table 3).

As already mentioned, the dose contribution above the ceiling and below the floor was estimated by considering two parallel slabs made of concrete. The proton beam

Table 6
Dose equivalent rate ($\mu Sv\,h^{-1}$) behind the walls and the floor of the accelerator room (see Figs. 1a and 1b) for the synchrotron beam loss sources

Position	Beam loss source								
	G1	G2	G3	G4	G5	G6	G7	G8	Total
Walls									
1	0.01	0.01	–	–	–	–	0.02	0.065	0.105
2	0.22	0.07	–	–	–	–	–	0.34	0.63
3	0.03	–	0.005	–	–	–	–	–	0.035
4	–	–	–	–	–	–	–	–	–
5	–	–	–	–	–	–	–	–	–
6	0.005	0.12	0.02	–	–	–	–	–	0.145
7	–	–	0.13	–	–	–	–	–	0.13
8	–	–	0.005	–	–	–	–	–	0.005
9	–	–	0.012	0.13	0.04	0.01	–	–	0.192
10	–	–	–	0.23	0.15	0.04	–	–	0.42
Floor									
201	0.01	0.002	–	–	–	0.01	0.15	0.14	0.312

Table 7
Dose equivalent rate ($\mu Sv\ h^{-1}$) behind the walls and the floor of the accelerator room (see Figs. 1a and 1b) for various beam loss sources

Position	Beam loss source								
	G	I	J	K1	K2	K3	L	M + N	Total
Walls									
1	0.105	0.063	–	–	–	0.04	–	–	0.208
2	0.63	1.38	–	2.20	–	–	–	–	**4.21**
3	0.035	0.19	–	–	0.04	–	–	–	0.265
4	–	–	–	–	0.61	–	–	–	0.61
5	–	–	–	–	–	–	–	–	–
6	0.145	0.032	–	–	–	–	–	–	0.177
7	0.13	–	–	–	–	–	1.39	–	**1.52**
8	0.005	–	–	–	–	–	0.04	–	0.045
9	0.192	–	0.25	–	–	–	–	0.6	1.042
10	0.42	–	0.95	–	–	–	–	2.20	**3.57**
Floor									
201	0.312	0.063	–	0.23	0.065	0.065	–	0.14	0.875

direction is parallel to the concrete slabs. The dose has been scored in different void cells 1 cm thick placed beyond the slabs. Various ceiling thicknesses have been considered, with fixed surface dimensions ($24 \times 16\ m^2$). The effect of each beam loss source in the accelerator room was studied. Table 8 gives the dose equivalent at various positions above the ceiling for different thicknesses. The contributing sources of beam loss are indicated for each position. For 120 cm thickness the dose equivalent rates were calculated both for 1 and 1/16 occupancy factors. This was done to take into account the possibility of having office space above the accelerator room. In this case a ceiling 200 cm thick is needed instead of 120 cm. It should be noted that at three positions (101, 104 corresponding to the beam extraction systems and 108, in bold in the table) the dose limit is exceeded in the case of 200 cm thickness. The effect of optional local shields will be discussed in the following. The dose equivalent in the environment under the synchrotron room level (position 201 in Fig. 1b and in Table 6 and Table 7) is below the limiting value with the chosen floor thickness (160 cm).

The concrete walls are obviously largely sufficient to shield the de-excitation photons produced in an iron target, whose energy distribution was determined in the simulations described in Section 4. Nevertheless a simulation considering the real room geometry and the beam loss source G1 (see Table 1) was also carried out to study the effect of the prompt gamma rays produced by neutron interactions in the walls. The resulting dose equivalent rates at various positions are reported in Table 9. It should be noted that the ratio between these values and the corresponding neutron dose equivalent varies from 0.5% at position 2 to 2.5% at position 201 below the floor. It is quite difficult to compare the results of the present work with those reported in the fairly scarce literature on this topic. In Refs. [34,35] the ratio of the photon to neutron dose equivalent was found to be of a few percent. It should be mentioned that the simulations performed in Ref. [34] refer to monoenergetic neutrons (in the energy range from 50 to 400 MeV) impinging on a slab of silicon dioxide plus 5% water content by weight. In the same reference only photons from neutron capture were considered. Ref. [35]

Table 8
Dose equivalent rate ($\mu Sv\ h^{-1}$) above the ceiling of the accelerator room for various beam loss sources (see Figs. 1a and 1b)

Position	Beam loss source	120 cm thickness occupancy factor 1	120 cm thickness occupancy factor 1/16	180 cm thickness occupancy factor 1	200 cm thickness occupancy factor 1
101	G1 + G2 + I	13	0.812	2.51	**1.21**
102	G3 + L	1.86	0.116	0.33	0.175
103	G4 + G5 + M + N + J	9.53	0.596	1.45	0.98
104	G5 + G6 + J	15.91	0.994	3.11	**1.495**
105	G1 + G8 + I + K	6.16	0.385	1.28	0.765
106	K	1.38	0.086	0.027	0.13
107	G7 + G8	2.55	0.159	0.435	0.22
108	G1 + G2 + G8 + I	15.11	0.944	2.75	**1.615**
109	G7 + K	3.38	0.211	0.64	0.345

Table 9
Photon dose equivalent rate ($\mu Sv\ h^{-1}$) behind the walls and the floor of the accelerator room (see Fig. 1b) for the synchrotron beam loss source G1

Position	Photon dose equivalent rate
Walls	
1	0.015×10^{-2}
2	0.106×10^{-2}
3	0.014×10^{-2}
4	–
5	–
6	0.15×10^{-2}
7	–
8	–
9	–
10	–
Floor	
201	0.025×10^{-2}

considers concrete shielding of monoenergetic neutrons in the energy range from 15 to 75 MeV, treating gamma ray production below 15 MeV. Photon measurements below single and combined shields of ordinary and heavy iron-loaded concrete (thickness between 0.8 and 2 m) and sand (thickness 3 m) were performed at various positions around a 7 GeV proton synchrotron [13]. A mean photon to neutron dose ratio of 0.16 with a standard deviation of 0.03 was found.

Iron was chosen as the material used to investigate the effect of local additional shields to be placed around the more intense sources in the real geometry. The shielding properties of iron were studied in Ref. [12], showing its effectiveness for neutrons above 1 MeV. A hollow iron sphere, 10 cm thick, with an inner radius of 40 cm was placed around the source corresponding to the beam extraction (I in Table 1). The resulting lateral contribution of the dose equivalent behind the shield is negligible, while in the forward direction it lowers from 1.38 $\mu Sv\ h^{-1}$ (see Table 7) to 0.87 $\mu Sv\ h^{-1}$ if the fixed beam treatment room (position 2 in Fig. 1b) is considered. The same value reduces to 0.63 $\mu Sv\ h^{-1}$ with an iron shield 20 cm thick.

A similar set of simulations was performed for the source K1, showing that in the fixed beam treatment room the dose equivalent rate lowers from 2.20 $\mu Sv\ h^{-1}$ (see Table 7) to 1.00, 0.40, 0.31 $\mu Sv\ h^{-1}$ with iron shields 20, 30, 40 cm thick respectively. The effect of an iron shield 20 cm thick placed around the sources at the extraction point and along the beam transfer line was also investigated for the ceiling. The results are given in Table 10.

Finally, a reference accident was simulated by a 250 MeV, 28 nA proton beam impinging on a concrete slab 250 cm thick for 200 ms (the extraction time for one synchrotron pulse). The total dose equivalent behind the shield was estimated 0.5 μSv. In the case of a complete beam loss on iron, the dose equivalent can be estimated from the results

Table 10
Dose equivalent rate ($\mu Sv\ h^{-1}$) above the 200 cm ceiling (occupancy factor 1) with a local iron shield around the beam extraction systems (H and I in Table 1) and the beam transfer line position K1

Position	Without local shield	With iron (thickness 20 cm)
108	1.615	0.53
104	1.495	0.60

discussed above. As an example, if the entire beam is lost at point K1 the dose equivalent in the fixed beam treatment room would be 0.8×10^{-2} μSv.

6. FLUKA shielding simulations

The calculations with FLUKA were subdivided into two parts: shielding of neutrons from the synchrotron inside the accelerator room; and shielding of neutrons from the sources localised inside the treatment rooms. The contribution of the photon dose equivalent was neglected, considering the low values found when using the LCS simulations.

6.1. Accelerator room: synchrotron source

FLUKA calculations for the accelerator room were carried out by only considering the source from the synchrotron. Being conducted in an analogous manner, particle transport was very similar to that of LCS, though some changes were made in the definition of the problem. On one hand, the real concrete mixture was used, since all the elements are available in the FLUKA neutron cross sections library; on the other hand, a description of the real geometry was too burdensome with this code and a simplified one was adopted. No appreciable effects were expected on the shield dimensioning and these assumptions were confirmed by the comparison of the results of the two codes. Differently from the LCS simulations, in which a proton beam impinging on an iron target was simulated, neutron sources with the double differential distributions calculated for the employed target material were considered.

As far as protons are concerned, the beam losses from the synchrotron were first localised at the dipole positions, as discussed in Section 5 for the LCS simulations. In a second step the beam losses, and consequently the neutron sources, were distributed along one half of the ring, with a strength of half of the full one. An equal neutron emission probability and the previously calculated angular distribution was attached at each point of the ring with the polar axis perpendicular to the forward wall, as shown in Fig. 7.

Care was taken in choosing the area where the neutron fluence in order to optimise the accuracy of the results and

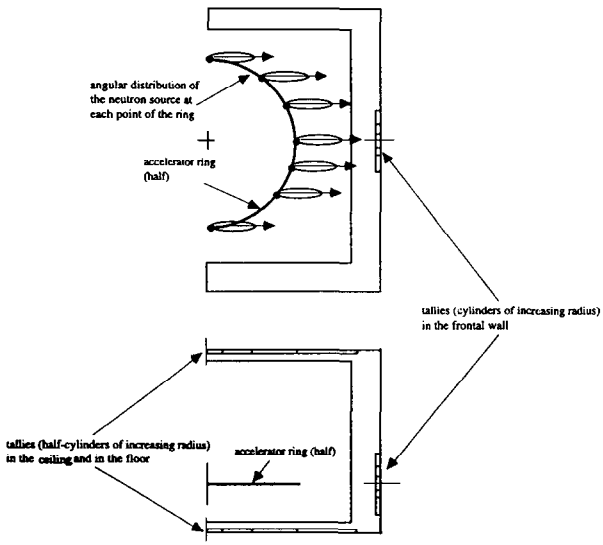

Fig. 7. Sectional views of the geometry adopted in the FLUKA calculations of the dose equivalent beyond the walls, floor and ceiling of the accelerator room.

reach an acceptable statistics and computing time was to be scored. Concentric surface tallies of increasing area were therefore used (see Fig. 7). The tallies referring to the forward wall were centred on the polar axis of the source at the closer point. The maximum dose equivalent position was investigated beyond the ceiling and the floor, as it is shifted with respect to the centre of the accelerator ring. Therefore, the dose equivalent behaviour with respect to the tally dimension and the concrete thickness was calculated for the forward wall, the ceiling and the floor. A very strong dependence on the tally dimension, dramatically decreasing with increasing scoring area, was observed for the forward wall. This effect was smaller for the ceiling and the floor, where a smoother behaviour of the dose equivalent with the tally dimensions was observed, therefore allowing larger scoring areas and better statistics. The final results, reported in Table 11, are consistent with those calculated with LCS.

6.2. Treatment and experimental rooms

Calculations with FLUKA were performed for all the rooms around the accelerator room. The shield dimensioning was ruled by the internal source and by the contribution from the accelerator or other rooms. No maze or inhomogeneity were considered at this stage of the calculations. A description is given below, identified by the same letters as Table 1.

Table 11
Maximum thicknesses (m) required for the accelerator room barriers, considering the synchrotron beam losses

	Thickness [m]
Walls	2.5
Ceiling	1.2
Floor	1.4

6.3. Isocentric gantry room

Losses were expected to be about of 50% of the beam in the patient (H_2O), about 45% in the collimator (Cu) and about 5% in the beam transfer line (Fe). The resulting neutron sources (neutrons per second) were 8.8×10^8, 6.31×10^9 and 5.41×10^8 respectively. It was assumed that the sources are directed toward the floor for 40% of the time, from left to right for 20%, from right to left for 20% and to all other directions for the remaining 20%. This last contribution was conservatively taken into account by increasing the forward component of the other three gantry directions by 20%.

A large set of calculations was performed separately considering the sources, since the energy and angular distributions are different for each material. The dose outside the room was calculated by adding the lateral and frontal contributions, depending on the orientation of the source with respect to the wall to be dimensioned. At present no evaluation for the floor has been made. The same tally optimisation was adopted as for the accelerator room. The neutron dose equivalent behind a concrete slab 50 cm thick from a 250 MeV proton beam impinging on a water target 27 cm thick increases by 9% if a proton scattering foil of lead is taken into account.

The results are summarised in Table 12, for two occupancy factors. Losses from copper and water give rise to doses of the same order of magnitude, while the effect of the losses from the transfer line is negligible for these thicknesses. The forward contribution is predominant compared with the lateral contribution and with that from

Table 12
Required shielding for the treatment and experimental rooms

		Occ. factor 1/16 thickness [m]	Occ. factor 1 thickness [m]
Walls	301	2.5	3.5
	302	2.5	3.5
	303	2.5	3.5
	304	2–2.5	3–3.5
	305	2.5–3	>3.5
	306	3	>3.5
	307	2.3	3
	308	2.3	3
Ceiling	401	2–2.5	3–3.5
	402		2
	403	0.5	1.8
	404	0.5	2
Floor	501	2.5–3	>3.5

losses in the synchrotron room; therefore the initial assumption that the source is directed towards any of the walls for 20% of the time rules the dimensioning of the walls. A less stringent hypothesis can bring the required thicknesses to a significant decrease. A revision of the occupancy factors and the use of additional local shields can be regarded as another way of reducing the fixed structure.

6.4. Fixed horizontal and vertical beam room

As for the gantry room, beam losses are likely to happen in the patient (H_2O,50%), in the collimator (Cu, 45%) and in the beam transfer line (Fe, 5%). The source was directed toward the floor for 50% of the time, while for the remaining time it was directed towards the wall separating the treatment room from the access corridor. The calculation was performed as previously described for the gantry room and the final results are reported in Table 12. No conservative assumptions were made and a reduction on the required thicknesses can be achieved by means of a revision of the occupancy factors and with the addition of local shields.

6.5. Experimental room

Losses are for 80% of the time in tissue equivalent material (H_2O) and for 20% in the collimator (Cu). The beam impinges on the target at 45° with respect to the accelerator room wall. The set of calculations already performed for the other rooms permitted the extrapolation of previous results; the required thicknesses are reported in Table 12. The Table also shows the effect of a reduction of the occupancy factor.

6.6. Horizontal beam treatment room

Losses are from beams of different energies, 70 MeV and 250 MeV, but the calculation was based on neutrons produced by the highest energy protons. Losses are in the patient (H_2O, 50%), in the collimator (Cu, 45%) and in the beam transfer line (Fe, 5%). The beam is perpendicular to the accelerator room wall. Results are given in Table 12 for two occupancy factors.

7. Discussion and conclusions

The LCS results were compared with the data of Refs. [6,36], resulting from the Monte Carlo simulations, and with the experimental data of Ref. [14]. In these works the neutron dose attenuation is fitted by the following exponential function, valid for shield thicknesses above 110 g cm^{-2}:

$$Dr^2 = SD_0\exp(-d/\lambda), \tag{2}$$

where D (Sv h^{-1}) is the dose beyond the concrete shield; r (m) is the distance from the neutron source; S (protons h^{-1}) is the proton beam intensity; D_0 (Sv m^2 proton^{-1}) is the source term; d (g cm^{-2}) is the shield thickness; λ is the average attenuation length.

The comparison was carried out by extrapolating these parameters from the simulation results for better evidence. Both lateral and forward shieldings were considered. The results of the simulations with the sources in position G1 (forward direction) and G3 (lateral direction) are compared with the literature data in Table 13. It should be mentioned that in Ref. [36] copper was considered as target material. Moreover, the dose attenuation was estimated with a monoenergetic parallel neutron beam impinging on a concrete slab. Ref. [6] concentrates on lateral shielding considering an iron target. The experimental results reported in Ref. [14] refer to 230 MeV protons impinging on an iron target with the same dimensions considered in the present work.

Table 13 shows that the results of the present work and the literature data agree within a factor 2. The dose values beyond a 250 cm thick concrete shield were estimated here considering the parameters given in the quoted literature referring to Eq. (2), for the sources in position G1 and G3.

As a further result of the LCS simulations performed in the present work, it should be mentioned that calculating a neutron shield by scoring the neutron fluence on fictitious

Table 13
Summary of shielding parameters calculated in the present work (LCS) and by other authors

	Forward shielding			Lateral shielding		
	D_0 [Sv m^2] per proton	λ [g cm^{-2}]	Dose beyond 250 cm concrete shield [μSv h^{-1}] source G1 (r = 15.6 m)	D_0 [Sv m^2] per proton	λ [g cm^{-2}]	Dose beyond 250 cm concrete shield [μSv h^{-1}] source G3 (r = 5.8 m)
Present work	**11.1×10^{-15}**	**86.2**	**0.22**	**4.0×10^{-15}**	**54.6**	**0.012**
Ref. [36][a]	3.36×10^{-15}	95.3	0.13	0.66×10^{-15}	73.0	0.028
Ref. [6]				0.6×10^{-15}	78	0.042
Ref. [14][b]	7.8×10^{-15}	89.1	0.65	0.76×10^{-15}	51.9	0.010

[a] Copper target.
[b] Concrete density 1.88 g cm^{-3}.

surfaces inside a thick concrete slab may give rise to an overestimation, due to the reflecting effect of the material beyond the scoring surface. The dose equivalent in the forward direction calculated with the simulation of the real room geometry with the source G1 is 0.22 $\mu Sv\,h^{-1}$ and 0.76 $\mu Sv\,h^{-1}$ beyond a 250 cm thick wall and on a surface at 250 cm inside a 400 cm thick wall, respectively (see Table 5 and position 2 referring to source G1 in Table 6).

On the other hand, a comparison between FLUKA and the semiempirical calculations, for the environments outside the accelerator room, shows that the semiempirical results were not as conservative as expected for sources frontally impinging on the barriers, while they were higher for lateral shields.

Acknowledgments

The authors thank Alberto Fassò (CERN, Geneve, Switzerland) and Alfredo Ferrari (INFN, Milano, Italy) for their useful advice and Paola Tabarelli (Università di Bologna, Italy) for her contribution to some Monte Carlo simulations. The authors are also indebted to Richard E. Prael (Los Alamos National Laboratory) for making the LCS code available and the experimental data on neutron yields and to the Referee for his very useful comments.

References

[1] U. Amaldi and M. Silari, eds., The TERA Project and the Centre for Oncological Hadrontherapy (INFN, Frascati, Italy, 1994).
[2] G. Arduini, R. Leone, R.L. Martin, S. Rossi and M. Silari, Nucl. Instr. and Meth. A, in press.
[3] G. Arduini, A. Bolshakov, R.L. Martin, K.K. Onosovski and M. Silari, Emittance and Time Structure of the Beam Extracted by Charge-Exchange from a H^- Synchrotron, to be published.
[4] G. Arduini, R.L. Martin, S. Rossi and M. Silari, Nucl. Instr. and Meth. A 346 (1994) 557.
[5] S. Agosteo, G. Bodei, R. Leone and M. Silari, in: Hadrontherapy in Oncology, Excerpta Medica, International Congress Series 1077 (1994) p. 525.
[6] K. Tesch, Radiat. Prot. Dosim. 11 (1985) 165.
[7] M. Awschalom, FNAL-TM-1354, Fermi National Accelerator Laboratory, Batavia, IL USA (1987).
[8] H. Dinter, K. Tesch and C. Yamaguchi, DESY 88-136, Hamburg, Germany (1988).
[9] W.K. Hagan, B.L. Coburn and T.W. Armstrong, Nucl. Sci. Eng. 98 (1988) 272.
[10] J.M. Zazula and K. Tesch, Nucl. Instr. and Meth. A 286 (1990) 279.
[11] J.M. Zazula and K. Tesch, Nucl. Instr. Meth. A 300 (1991) 164.
[12] K. Tesch, J.M. Zazula, Nucl. Instr. and Meth. A 300 (1991) 179.
[13] D. Dworak, K. Tesch and J.M. Zazula, Nucl. Instr. and Meth. A 321 (1992) 589.
[14] J.W. Siebers, P.M. DeLuca Jr., D.W. Pearson and G. Coutrakon, Nucl. Sci. Eng. 115 (1993) 13.
[15] R.H. Thomas and G.R. Stevenson, Radiological Safety Aspects of the Operation of Proton Accelerators, Technical Report Series No. 283 (IAEA, Vienna, 1988).
[16] International Commission on Radiological Protection, ICRP Publication 60 (Pergamon, 1990).
[17] R.E. Prael, H. Lichtenstein, LA-UR-89-3014, Los Alamos National Laboratory (Los Alamos, New Mexico, USA, 1989).
[18] A. Fassò, A. Ferrari, J. Ranft and P.R. Sala, Proc. 4th Int. Conf. on Calorimetry in High Energy Physics, La Biodola, Italy, 1993, eds. A. Menzione and A. Scribano (World Scientific, 1993) p. 493.
[19] C. Wuzhong, GSI-92-24 (1992).
[20] A. Rindi, LBL-4212 (1975).
[21] A.V. Daniel et al., JINR Dubna E1-92-174 (1992).
[22] W.F. Ohnesorge, H.M. Butler, C.B. Fulmer and S.W. Mosko, Health Phys. 39 (1980) 633.
[23] F. Clapier and C.S. Zaidinis, Nucl. Instr. and Meth. 217 (1983) 489.
[24] G.A. Petitt et al., Phys. Rev. C 32 (1985) 1572.
[25] V.E. Aleinikov, A.P. Cherevatenko, F.B. Clapier and V.I. Tsovbun, Rad. Prot. Dosim. 11 (1985) 245.
[26] J.B. McCaslin, P.R. LaPlant, A.R. Smith, W.P. Swanson and R.H. Thomas, IEEE Trans. Nucl. Sci. NS-32 (1985) 3104.
[27] L. Schmieder, D. Hilscher, H. Rossner, U. Jahnke, M. Lehmann, K. Ziegler and H.H. Knitter, Nucl. Instr. and Meth. A 256 (1987) 457.
[28] L. Fiore et al., Phys. Rev. C 41 (1990) R419.
[29] T. Kato and T. Nakamura, Nucl. Instr. and Meth. A 311 (1992) 548.
[30] B.B. Back, Nucl. Instr. and Meth. B 74 (1993) 527.
[31] H.R. Schelin et al., Nucl. Sci. Eng. 113 (1993) 184.
[32] M.M. Meier, C.A. Goulding, G.L. Morgan and J.L. Ullmann, Nucl. Sci. Eng. 104 (1990) 339.
[33] E.A. Belogorlov, V.T. Golovachik, V.N. Lebedev and E.L. Potjomkin, Nucl. Instr. and Meth. 199 (1982) 563.
[34] R.G. Alsmiller, F.R. Mynatt, J. Barish and W.W. Engle, Nucl. Instr. and Meth. 72 (1969) 213.
[35] R.W. Roussin, R.G. Alsmiller and J. Barish, Nucl. Eng. Design 24 (1973) 250.
[36] T.H. Braid, R.F. Rapids, R.H. Siemssen, J.W. Tippie and K. O'Brien, IEEE Trans. Nucl. Sci. NS-18 (1971) 821.